Institute of Paper Science and Technology
Atlanta, Georgia

IPST TECHNICAL PAPER SERIES

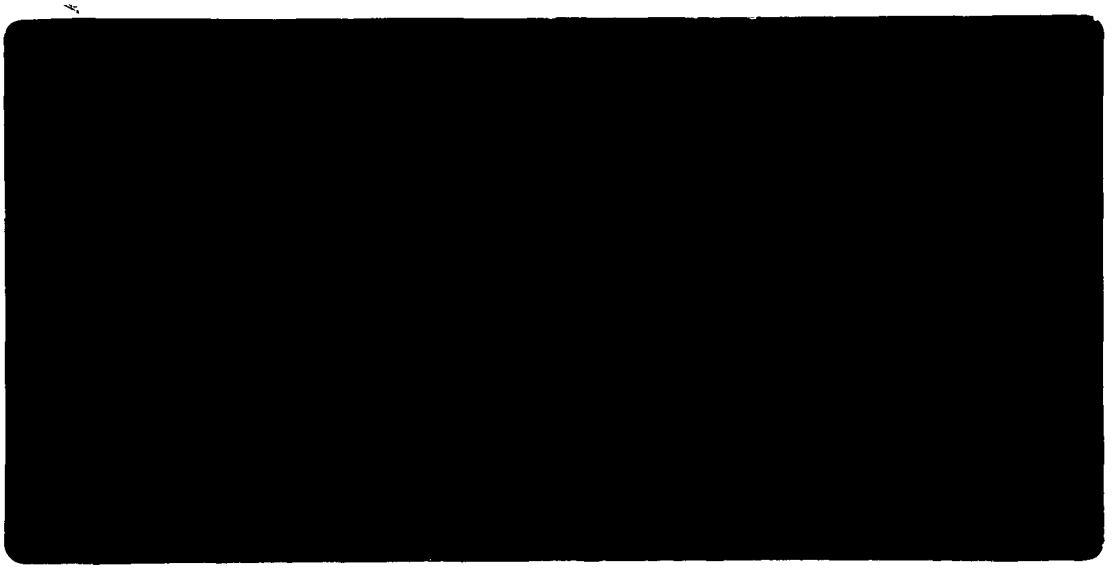

NUMBER 437

EFFECTS OF HEATING MODE ON ROLL DURABILITY AND EFFICIENCY OF IMPULSE DRYING

D.I. ORLOFF, G.L. JONES, AND P.M. PHELAN

APRIL 1992

Effects of Heating Mode on Roll Durability and Efficiency of Impulse Drying

D.I. Orloff, G.L. Jones, and P.M. Phelan

Submitted to
National Heat Transfer Conference
August 1992
San Diego, CA

EFFECTS OF HEATING MODE ON ROLL DURABILITY AND EFFICIENCY OF IMPULSE DRYING

David I. Orloff
Professor

Gary L. Jones
Associate Professor

Paul M. Phelan
Assistant Scientist

Institute of Paper Science and Technology
Atlanta, Georgia, USA

Abstract

Vacuum deposited surface thermocouples have been used to measure heat flux during impulse drying with ceramic coated press surfaces. The measured heat flux was used as a boundary condition to a numerical heat transfer model to predict internal press roll temperatures and roll heating efficiency. The simulations demonstrate that maximum roll durability and heating efficiency can be realized when the press roll is externally heated and when internal roll temperatures are maximized.

Nomenclature

Units (unless noted): time (s), distance (m), mass (kg), heat (joules), power (watts), temperature (K).

C	=	circumference
Cp	=	heat capacity
d	=	layer thickness
E	=	energy transfer (J/cm revolution)
e	=	electrical conductivity
f	=	adjustable parameter
H	=	magnetic flux
h	=	heat transfer coefficient
K	=	proportional gain
k	=	thermal conductivity
n1,n2,n3	=	number of finite increments in layers 1,2,3
p	=	relative magnetic permeability
Q	=	heat flux
R	=	radial position
r	=	radial coordinate
RPS	=	rotational frequency
S	=	surface distance
T	=	interfacial temperatures
t	=	time
T_e	=	temperature error (for control)
V	=	linear surface velocity
v	=	void fraction
Y	=	interior temperature
z	=	cross machine coordinate
α	=	thermal diffusivity
β	=	heat capacity coefficients
Δr	=	radial increment
γ	=	thermal diffusivity coefficients
ε	=	thermal emissivity
λ	=	numerical stability parameter
μ_o	=	permeability of free space
ρ	=	density
σ	=	Stephen-Boltzmann constant
τ	=	time constant
τ_I	=	reset time constant
θ	=	angular coordinate
ω	=	angular frequency

Subscripts

a	=	absolute
air	=	air
c1	=	outer ceramic layer
c2	=	inner ceramic layer
h	=	heating zone
i	=	index
in	=	inside
ind	=	induction zone
j	=	time step
k	=	layer index
l	=	energy zone
1,10,1c	=	lamp zone
l1,2	=	heat loss zones
o	=	outside
oil	=	heat transfer medium, oil
p	=	paper
r	=	radiation
s	=	metal
so	=	solid
0	=	entrance to the nip
1,2,3,4	=	interfacial position

Superscripts

t	=	temporary

Introduction

In current practice, energy intensive evaporative drying is used to dry paper. Early research showed that a significant fraction of that energy could be saved by impulse drying (Lavery, 1988). Unfortunately, implementation of the technology was halted as impulse drying induced defects termed "sheet delamination" (Crouse, 1989).

Ongoing research at the Institute of Paper Science and Technology has focused on process design modifications that eliminate sheet delamination. By replacing metallic press surfaces with low heat capacity, low thermal conductivity ceramics, sheet delamination can be avoided (Orloff, 1991; Orloff, 1992; Orloff and Lindsey, 1992). While additional research is underway to expand the operating range of these ceramics, the present ceramic design will be evaluated on a pilot-scale press in the near future. This paper focuses on a number of design issues relating to the demonstration of impulse drying on a commercially configured press section.

Fig. 1 shows a crown-compensated extended-nip press configured with a ceramic coated press roll. In the impulse drying mode, the hydrostatic support element will load the roll shell, which revolves at a speed of 760 m/min, to a peak pressure of 6.2 MPa. An oil film between the element and the moving shell provides lubrication and acts as a heat sink for heat loss to the interior of the roll. An extended nip of 40 ms duration may be developed by using an elongated press shoe.

Wet paper carried on a felt enters the extended nip at 40% dryness at location A and leaves the nip at 60% dryness at location C. The roll is heated in a zone from location D to E such that the temperature of the roll surface at the entrance to the nip at A is 370°C.

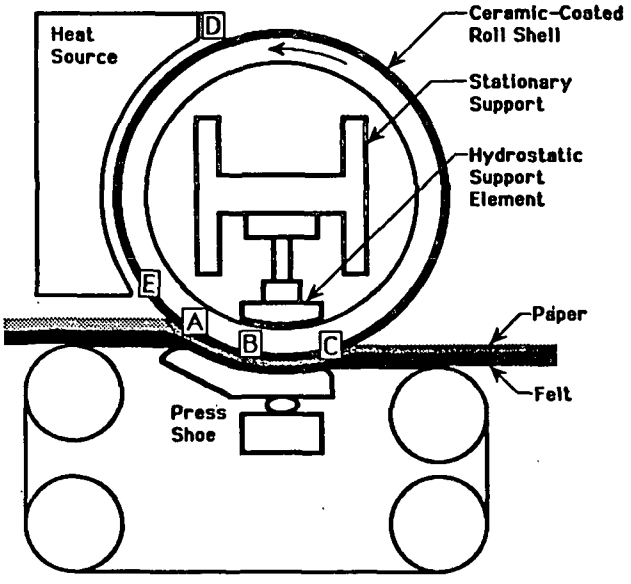

Figure 1. Crown compensated extended nip press with ceramic coated impulse drying press roll.

With impulse drying, water is pressed out of the sheet by a combination of mechanisms that enhance normal wet pressing. These include a reduction in liquid water viscosity and increased fiber conformability due to higher sheet temperatures, and increased internal hydraulic pressures resulting from vapor formation at the interface of the press roll and the sheet.

Incremental improvements in water removal achieved by raising the roll temperature far exceed gains that would be expected based on evaporation. Hence, impulse drying improves water removal while saving evaporative energy. To achieve this energy savings in practice, process equipment must be designed to facilitate efficient roll heating. This means that the ceramic coated press roll should be designed to maximize roll heating efficiency.

As the ceramic coatings will be applied to a steel or cast iron shell, the ceramic coating and roll heating technology should also be chosen to minimize thermal stresses resulting from excessive temperature fluctuations at the ceramic/metallic interface.

A combined experimental and analytical research program was undertaken to address these design issues. The experimental work consisted of measurements of heat flux from the ceramic coating to the paper during impulse drying using a low mass, high response, vacuum deposited surface thermocouple. The analytical work consisted of the development of a numerical heat transfer simulation of the press roll using the experimental heat flux data as a boundary condition.

Experimental Measurement Of Heat Flux

Impulse Drying Simulation

Fig. 2 shows a schematic of the electrohydraulic press used to simulate impulse drying and to measure heat flux. The apparatus was designed to simulate the transient mechanical and thermal conditions experienced by paper during impulse drying. The electrohydraulic press simulated the expected pressure history that the sheet would experience in a commercial impulse dryer. Likewise, the thermal conditions were simulated using a platen having the same composition as the surface of the roll press and heating that platen to the operating temperature of the process. As the dominant direction of flow is out-of-plane, the electrohydraulic press was expected to provide an excellent simulation of the impulse drying process.

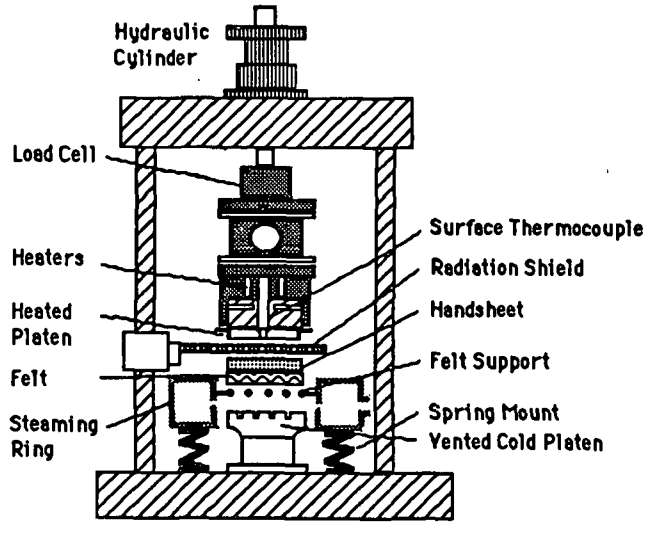

Figure 2. Schematic of the electrohydraulic press.

In the experiments, wet sheets of paper on felts were placed onto a wire felt support attached to a steaming ring. A radiation shield was automatically positioned between the heated platen and the sheet to reduce dry-out of the top surface of the sheet. Steam exiting from the ring flowed upward through the felt and the sheet. By controlling steam pressure and adjusting the steaming time, the initial temperature in the sheet was raised to 85°C.

Once the sheet was heated, the hydraulic system was activated to give a haversine pressure pulse of 40 ms duration and 6.2 MPa peak pressure. The temperature at the surface of the ceramic platen was recorded as a function of time during the impulse drying event. As the structure and thermal properties of the ceramic coating were known, heat flux to the paper sheet could be calculated as a function of time.

Ceramic Thermal Properties

The ceramic coating consisted of plasma sprayed zirconium oxide layers with controlled porosity. The surface layer was 0.05 mm thick with 7% porosity, while the inner layer was 0.38 mm thick with 15% porosity. Porous ceramics have thermal properties that are dependent on the properties of the solid ceramic, void fraction, and a material specific empirical constant, C', (Nielson, 1978; Batakis, 1985).

$$\rho = \rho_{so}(1-v) \tag{1}$$

$$Cp = Cp_{so} \tag{2}$$

$$k = \frac{k_{so}}{(1+C'v)} \tag{3}$$

$$\alpha = \frac{k}{\rho Cp} = \frac{\alpha_{so}}{(1-v)(1+C'v)} \tag{4}$$

To determine the properties of the two ceramic layers, three plasma sprayed zirconium oxide samples were prepared at three different void fractions. Void fraction was measured from cross-sectional micrographs. Specific heat and thermal diffusivity were measured by differential scanning calorimetry and a laser flash diffusivity method respectively. All thermal measurements were made by the Properties Research Laboratory of West Lafayette, Indiana.

The specific heat data were fit to a polynomial in temperature,

$$Cp_{so} = \sum_{n=0}^{3} \beta_n (T_a)^n \tag{5}$$

where the coefficients β_n in units of J/(g K) are given in the appendix.

The diffusivity data were scaled using Equation (4) and fit to the following polynomial in temperature.

$$\alpha_{so} = \sum_{n=0}^{4} \gamma_n (T_a)^n \tag{6}$$

A value of C' = 8.52 gave the best correlation of the data. The coefficients of Equation (6) to give α_{so} in units of cm^2/s are also shown in the appendix.

Thermocouple Design

Accurate calculations of heat flux require accurate surface temperature measurements during the impulse drying event. Design requirements for a thermocouple for use with a ceramic coating include:

1) The thermocouple must be flush with the ceramic surface.
2) The thermocouple must be constructed to assure one-dimensional heat flow.
3) The response time must be fast, 10-20μs.
4) There must be no thermal contact resistance between the thermocouple and the ceramic.
5) The thermocouple must have low mass.

Preliminary experiments show that ribbon thermocouples stretched across the ceramic surface can yield questionable heat flux data due to failure to meet the last two conditions (Orloff, 1991). In this work, all of the criteria were met by using a small vacuum deposited thermocouple which was applied directly to the ceramic surface.

Because alloys do not deposit uniformly, pure copper and nickel were chosen as the thermocouple components. This choice gave the best millivolt response of commonly available materials. To make the thermocouple, the leads were mounted in the platen with a separation of 1.5 mm with the exposed ends flush with the ceramic surface. A copper film was deposited over the copper lead. Then a nickel film was deposited over the copper film and nickel lead yielding a thermocouple having a thickness of 0.001 mm and a surface area of 3 mm^2.

A copper/nickel reference junction was used in an ice bath. The completed thermocouple was calibrated using known temperatures over the range of temperatures expected in the impulse drying experiments. The thermocouple was expected to be accurate within 1°C.

Heat Flux Calculations

For one-dimensional heat flow in a semi-infinite solid with constant thermal properties, constant initial temperature, and a time variant surface temperature, the heat flux at the surface may be expressed (Giedt, 1955) as,

$$q(t) = \frac{2k}{\sqrt{\pi\alpha}} \sum_{i=1}^{n} m_i \left[(t_n - t_{i-1})^{1/2} - (t_n - t_i)^{1/2} \right] \tag{7}$$

The local slopes, m_i, were calculated using a seven point least squares routine centered on the desired data point.

$$m_i = \frac{7 \sum_{n=i-3}^{i+3} t_n T_n - \sum_n t_n \sum_n T_n}{7 \sum_n (t_n)^2 - \sum_n t_n \sum_n t_n} \tag{8}$$

The initial assumption of constant physical properties was relaxed in that it was assumed that the properties were 'locally' constant. It was further assumed that the platen was a semi-infinite ceramic solid with a constant average void fraction, v = 0.1. Cumulative energy transfer was calculated from the heat flux by a trapezoidal integration technique.

$$E_i = E_{i-1} + \Delta t \frac{(q_i + q_{i-1})}{2} \tag{9}$$

Results Of Heat Flux Measurements

Sheets of single-ply linerboard, at a basis weight (oven-dried) of 205 g/m^2 were formed on a slow speed web former from virgin southern pine kraft which had been refined to 650 ml Canadian Standard Freeness. The sheets were pressed to 42% solids and preheated to 85°C prior to impulse drying on the hydraulic press. Impulse drying was simulated for the case of a 40 ms nip at a peak pressure of 6.2 MPa. Ingoing ceramic surface temperatures ranged from 150°C to 400°C

Typical platen surface temperature versus time data at three different ingoing platen surface temperatures are shown in Fig. 3. Heat flux calculated from that data are shown in Fig. 4.

As had been previously observed (Orloff, 1991), heat flux was only dependent on the initial temperature of the ceramic surface. Fig. 5 shows a correlation of heat flux divided by the difference between the initial ceramic surface temperature, and the initial sheet temperature as a function of time. Equation (10) expresses that relationship in terms of a polynomial in time.

$$\frac{Q_{nip}}{(T_0 - T_p)} = +0.0074 - 7.03t - 70.6t^2 - 1.44\times10^4 t^3 + 8.73\times10^5 t^4 - 1.06\times10^7 t^5 \qquad (10)$$

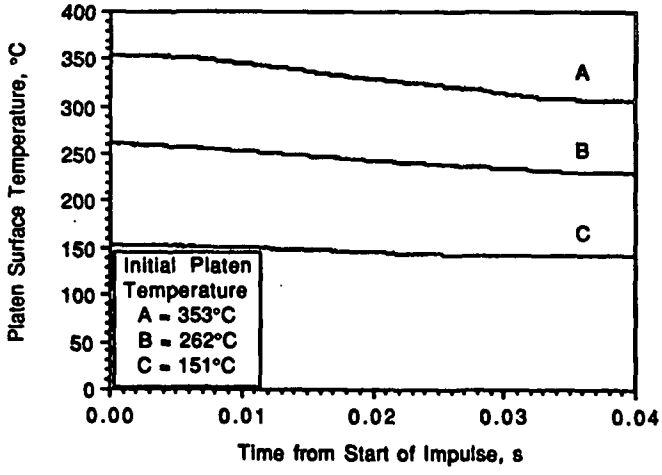

Figure 3. Platen surface temperature versus time during impulse drying.

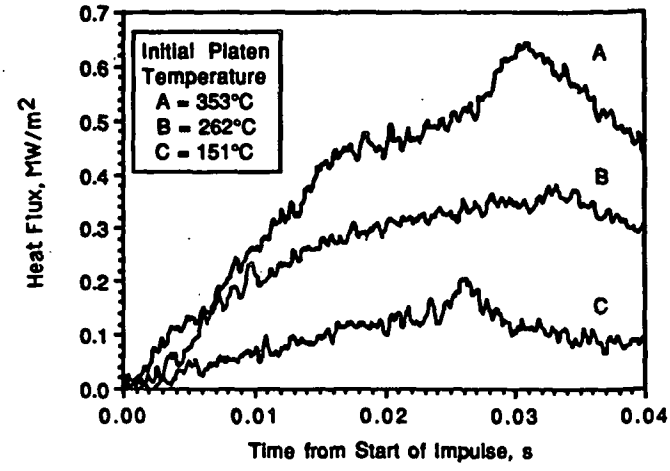

Figure 4. Heat flux versus time during impulse drying.

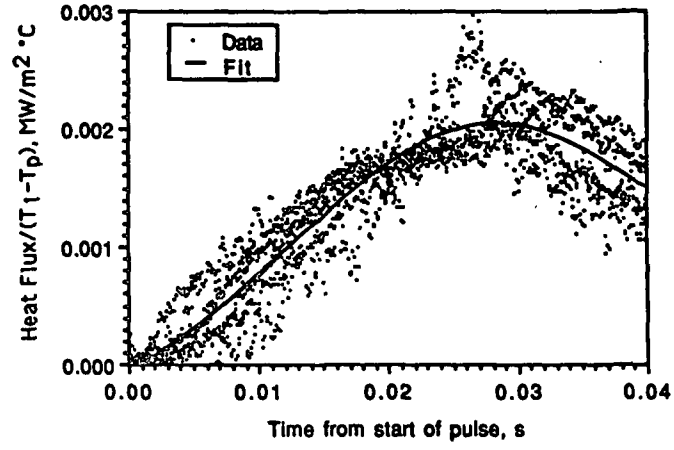

Figure 5. Heat flux correlation.

Numerical Heat Transfer Model

The heat transfer model was developed to determine the temperature profiles within the roll and the distribution of heat from the heat source to the nip, to the ambient environment, and to the internal heat transfer medium (oil).

The model was based on the roll structure shown in Fig. 6, consisting of two relatively thin layers of ceramic over a cylindrical metal (cast iron) shell approximately 0.1 m thick. At the commercial scale the roll will be in contact with a heat transfer medium to control and cool the inside temperature.

In the nip zone heat was transferred from the roll to the paper and the general direction of heat flow was from the interior of the roll toward the surface. Heat was added to the roll over a heating zone near the inlet to the nip to balance heat transfer to the nip and other heat losses and to return the surface temperature to a desired set point.

In the cylindrical coordinate system shown, the z or cross-machine direction was assumed to be infinite and heat transfer took place in the radial, r, direction. Rotation was in the θ direction. The transient model was based on an angular slice of the roll of arbitrary angular extent, $\Delta\theta$,

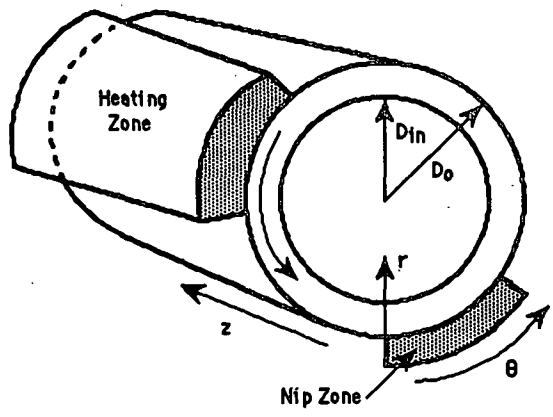

Figure 6. Roll geometry used in analytical model

rotating at a constant velocity, V, experiencing a transient heat flux at the outer surface and transferring heat to a heat transfer medium.

Heat was transferred to the roll in one of two ways: externally by infrared radiation or internally by magnetic induction. In both heating modes the heat flux was confined to a specific length of time corresponding to a specific circumferential distance as shown in Fig. 6. Based on the above assumptions the model was applied to a finite element of variable width or angular extent which depends on the variable time step as shown in Fig. 7. The differential element was exposed to a transient heat flux at the outer boundary or at the induction zone through each revolution.

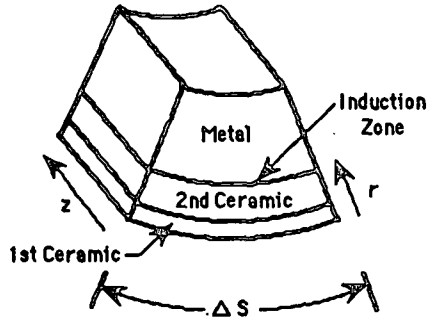

Figure 7. Multi-layer roll structure.

Conduction in the θ and cross machine (into the plane) or z directions was negligible because the thermal gradients in these directions were small relative to the radial direction. The relation between the variable change in surface distance, ΔS, and the variable time step, Δt, was

$$\Delta S = V\,\Delta t \tag{11}$$

The most general form of the energy balance for each layer reduces to the following transient one-dimensional heat conduction equation,

$$\frac{\partial T}{\partial t} = \alpha\left(\frac{\partial^2 T}{\partial r^2} + \frac{1}{r}\frac{\partial T}{\partial r}\right) + \frac{Q_{ind}}{\rho C_p} \tag{12}$$

The heat generation term, Q_{ind}, the rate of heat generation per unit volume of the roll, applies only to the induction heating mode. In the induction mode Q_{ind} was nonzero only over a thin layer between the inner ceramic and metal layers in which the magnetic field couples with the roll material. There was no heat generation within the ceramic.

The decay of magnetic flux, H, with radial distance, r, was a function of angular frequency, ω, relative magnetic permeability, p, and electrical conductivity, e.

$$H = H_0 \exp\left(-\frac{2r}{\tau_h}\right) \tag{13}$$

$$\text{where } \tau_h = \sqrt{\frac{2}{\omega p \mu_o e}} \tag{14}$$

At a frequency of 3000 Hz, the thickness of the induction layer, d_{ind} (cm), was defined as the distance over which H decays to 1/e of its initial value,

$$d_{ind} = \frac{920}{\sqrt{e\ p}} \tag{15}$$

Evaluation shows that this layer was less than the thickness of one finite thickness in the metal layer. Because the heat generation zone was very thin, heat generation was lumped into the boundary condition at the ceramic-metal interface.

In finite difference form Equation (12) becomes

$$\frac{\partial Y_i}{\partial t} = \alpha_i\left[\frac{(Y_{i+1}-2Y_i+Y_{i-1})}{\Delta r_k^2} + \frac{(Y_{i-1}-Y_{i+1})}{2\Delta r_k R_{ik}}\right] \tag{16}$$

Y_i was an interior temperature (as opposed to an interfacial temperature). The radial step size for each layer was fixed and was scaled to each layer thickness. R_{ik} was the radial distance to the ith element in the kth layer. The discretation of the three layers and boundary points are shown in Fig. 8.

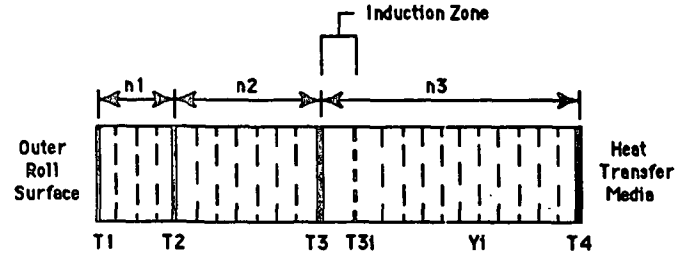

Figure 8. Finite difference.

The heat balance over each layer was subject to a flux boundary condition at each interface. For the outer ceramic layer, Q_{nip} (W/cm^2), was a function of position or, equivalently, time as given in Equation (10). T_0 was the surface temperature at the entrance to the nip, and T_p was the fixed initial sheet temperature of 85°C.

For the nip zone,

$$T_1 = Y_1 + \frac{Q_{nip}}{\frac{k_{c1}}{\Delta r_{c1}}} \tag{17}$$

Open zones between the nip and the lamp

For the two zones open to the air in which heat losses occur through convective and radiative heat transfer, the surface temperature was given by

$$T_1 = \frac{h_{air}T_{air} + \frac{k_{c1}}{\Delta r_{c1}} Y_1 + Q_{r_1}}{h_{air} + \frac{k_{r_1}}{\Delta r_{c1}}} \qquad (18)$$

where Q_r, the radiative heat flux, was given by

$$Q_r = -\epsilon\sigma (T_a^4 - T_{air}^4) \qquad (19)$$

The convective heat transfer coefficient, h_{air}, was given by

$$h_{air} = 4.0\text{x}10^{-3}\, k_{air} \sqrt{\frac{V}{C}} \qquad V < 15 \qquad (20)$$

$$h_{air} = 6.2\text{x}10^{-3}\, k_{air} \frac{V^{0.8}}{C^{0.2}} \qquad V \geq 15 \qquad (21)$$

where k_{air} was the thermal conductivity of air equal to 0.0260 W/m°K. The velocity, V, was defined in terms of the circumference, C, and the rotational frequency, RPS,

$$V = RPS\, C^2 \qquad (22)$$

The boundary condition in this zone was only approximate since the radiative heat flux was evaluated at the previous value of the surface temperature while the convective term was used to compute the surface temperature.

For the heating zone, the surface temperature was defined differently for each of the two heating modes. For external infrared roll heating, the surface temperature was given by

$$T_1 = Y_1 + \frac{Q_l}{\frac{k_{c1}}{\Delta r_{c1}}} \qquad (23)$$

where the effective lamp heat flux reaching the roll surface, Q_l, was given by an offset term and a PI controller algorithm defined as

$$Q_l = Q_{l0} + Q_{lc} \qquad (24)$$

Q_{l0} was defined in terms of an overall heat flux balance given by

$$Q_{l0} = -\frac{(E_{nip} + E_{l1} + E_{l2})}{A_o \tau_l} \qquad (25)$$

$$Q_{lc} = -K\left[T_e + \frac{1}{\tau_I}\int_0^t T_e\, dt\right] \qquad (26)$$

where the temperature error, T_e, was given by

$$T_e = T_0 - T_{sp} \qquad (27)$$

For the induction heating mode, heat was lost through the surface through convection and radiation. The surface temperature was defined through similar equations.

The second boundary condition for the interfacial temperature between the two ceramic layers was based on the equality of the heat flux at the interface, $r = R_1$,

$$k_{c1}\frac{\partial Y}{\partial r}\bigg|_{R_1^-} = k_{c2}\frac{\partial Y}{\partial r}\bigg|_{R_1^+} \qquad (28)$$

This condition was used to evaluate the interfacial temperature, T_2, as follows:

$$T_2 = \frac{k_{c1}\frac{Y_{n1-1}}{\Delta r_{c1}} + k_{c2}\frac{Y_{n1}}{\Delta r_{c2}}}{\frac{k_{c1}}{\Delta r_{c1}} + \frac{k_{c2}}{\Delta r_{c2}}} \qquad (29)$$

For the external infrared heating mode, the boundary condition between the ceramic and metal layers was based on the equality of heat flux at $r = R_2$, from which the interfacial temperature, T_3, becomes

$$T_3 = \frac{k_{c2}\frac{Y_{n2-1}}{\Delta r_{c2}} + k_s\frac{Y_{n2}}{\Delta r_s}}{\frac{k_{c2}}{\Delta r_{c2}} + \frac{k_s}{\Delta r_s}} \qquad (30)$$

For the induction heating case subscript 's' was replaced by 'ind'. An additional boundary was assigned to the end of the induction zone and an additional interfacial temperature, T_{3i}, was defined by applying the equality of flux at the interface between the induction zone and metal zone. The induction heat flux was assumed to be applied at the interface.

$$T_{3i} = \frac{k_s\frac{Y_{n2-1}}{\Delta r_i} + k_s\frac{Y_{n2}}{\Delta r_s} + Q_{ind}}{\frac{k_s}{\Delta r_i} + \frac{k_s}{\Delta r_s}} \qquad (31)$$

As with the external infrared heating mode, the induction heat flux was controlled by means of a feedback loop in which the base flux level was defined through an approximate overall energy balance. The total flux level was the sum of the base level and a correction based on the error detected by the feedback loop. The algorithm for the induction heat flux was the same as that used for the external infrared heating case described above.

The boundary condition at the metal-oil interface was defined in terms of a known interfacial temperature T_4.

Overall Heat Balances

Several overall heat balances were defined in order to quantify and compare the rate of heat addition, removal and flow from various sections of the roll. From these values it was possible to extract the thermal efficiency of the process.

The total energy transferred in the nip per unit roll width per revolution was

$$E_{nip} = C\sum_{j=0}^{jmax}\frac{k_{c1j}(T_{1j} - Y_{1j})}{\Delta r_{c1}}\Delta t_j \qquad (32)$$

For the heat transfer from the roll to the oil,

$$E_{oil} = -A_i\, k_s\sum_{j=0}^{jmax}\frac{(Y_{(n3-3)j} - T_4)\,\Delta t_j}{\Delta r_s} \qquad (33)$$

Other energy transfers were defined in a similar fashion.

An overall roll energy balance was defined as the total energy transferred in one revolution through the surface and metal-oil interfaces. The overall heat balances were then used to determine: the consistency of the flux calculations, overall energy closure and numerical accuracy, the net energy transferred to and from the ceramic, and the overall energy losses to the air and oil.

Numerical Algorithm

The heat transport equation in each layer was discretized in the r-direction in each layer in a fashion analogous to the method of lines. Each zone was assigned the same number of points. The size of each interval was thus proportional to the thickness of each layer. As described in the experimental section, the thickness of the cast iron layer was approximately 100 mm. Thus the thickness of each metal layer was approximately 10 mm while the thickness of the ceramic layers were approximately 0.08 mm each. The highly transient surface boundary condition was expected to cause the thermal gradients to vary rapidly both in time and space within the top layers of the roll. These high frequency variations require a disproportionate fraction of the points be located in the ceramic layers. As shown theoretically (Carnahan, 1969), if the dimensionless variable λ was given by,

$$\lambda = \alpha \frac{\Delta t}{(\Delta r)^2} \tag{34}$$

the minimum step for stability was,

$$\lambda \leq \frac{1}{2} \tag{35}$$

For the outer ceramic layer, $\alpha = 1 \times 10^{-6}$ m^2/s, and $\Delta r_1 = 0.076$ mm. Thus the minimum time step for stability and convergence was approximately,

$$\Delta t \leq 2.9 \times 10^{-3} \text{ seconds.} \tag{36}$$

The above criteria was based on an explicit representation of the time derivative. Larger time steps may be possible (i.e., lead to a stable convergent solution) for other approaches such as an implicit approach. Not only was the problem at hand nonlinear, it also contains nonlinear and time dependent boundary conditions and the above criteria may not be severe enough to assure stability or convergence. Thus for this general problem there was probably no exact method to assure convergence and stability. An analysis of the physical problem indicated that the rate of change of the temperature near the surface was three or four orders of magnitude larger than derivatives in the interior. In fact the derivatives were nearly zero in the interior of the cast iron zone due to a near cancellation of the temperature waves propagating into the solid.

This high variation in derivative magnitude and sign was indicative of a highly stiff system. Highly stiff systems normally require small and generally variable time steps due to the change in inherent stiffness with time. Another aspect of the problem was the inherent transience of the heat transfer process. The combination of cyclic heat addition and removal and the superposition of the control system makes the solution at best pseudo-steady for long times. Perhaps the best that can be expected was an approach to a steady oscillation in the temperature profiles for each cycle.

A wide variety of methods are available to solve the system of equations. These include the method of lines, Runge-Kutta methods of various orders, and various Gear methods. A novel semi-implicit variable time step method developed at the Institute was used because of its previously demonstrated stability and accuracy with other highly stiff systems. The method is only briefly summarized here and is described in detail elsewhere (Jones, 1990; Hart, 1991).

First a vector of trial increments Δy_i, was calculated based on the explicit evaluation of the derivatives with the temperature profile at the current position and time.

$$\Delta y_i = \Delta t^t \, f(y,\alpha) \tag{37}$$

where f was the derivative and Δt^t was a trial time step.

The derivatives were evaluated at the half-interval and a trial vector of time steps was determined.

$$\Delta t_i^t = \frac{f_i(\alpha_i, \overline{Y})}{\Delta Y_i^t} \tag{38}$$

where $\overline{Y}$ was the appropriate set of Y values at the half time interval. If all the trial Δt values were positive, the trial increment was feasible and the minimum time increment was selected. The final increments were then scaled based on the ratio of the minimum time step to the time step for each i. Thus the equation with the highest derivative determines the time step. Furthermore, the time step was consistent with an implicit set of changes in Y. If one or more of the time steps in the trial vector was negative, those trial steps were not feasible.

Any infeasible trial increment was reduced by a factor of two and a new trial vector was computed at the half interval. The process was repeated until a feasible set was determined.

The elapsed time was then incremented until a complete revolution was made. If the elapsed time exceeds the time per revolution, the minimum time step was set to the remaining time and the final increments were scaled based on this time step. If the time increment jumps the location from the nip zone into the air zone, there was no backward stepping to assure that the computations begin exactly at the transition between each zone. However, since the time steps were always several orders of magnitude smaller than the time in any zone, the resulting error was judged to be negligible.

Discussion of Numerical Results

Calculation Of Heat Flux

The method used to calculate heat flux from experimental surface temperature measurements assumed a semi-infinite ceramic of constant void volume. The more general numerical model, described in the previous section, was used to calculate temperature profiles and energy transfer based on correlated experimental heat flux data. In addition, a modified version of the numerical model used a test temperature profile to compare calculated heat flux from the two models. The similarity of the results, as shown in Fig. 9 and 10, suggest that the assumed uniform void volume of 0.1 was appropriate.

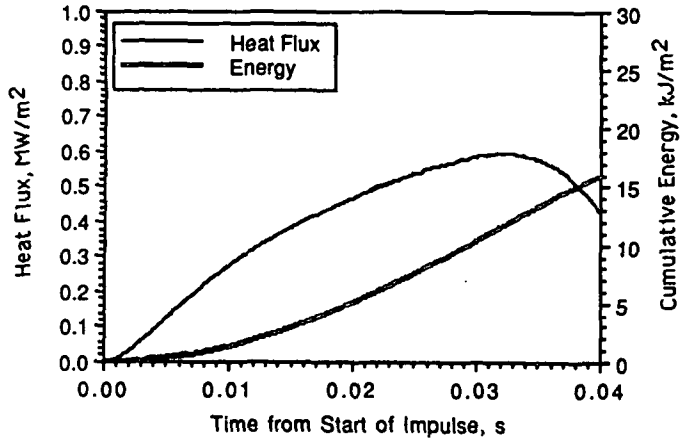

Figure 9. Heat flux calculated using infinite ceramic slab assumption.

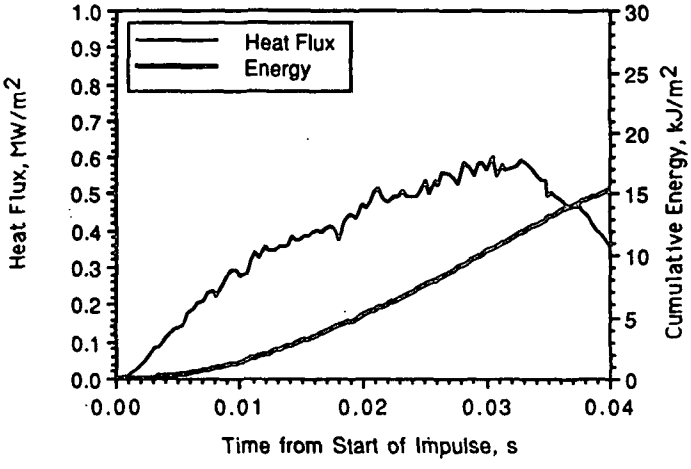

Figure 10. Heat flux calculated using analytical multi-layered ceramic model.

As a further test, the numerical model was used to compute temperature profiles in the two layer ceramic coated steel platen as a function of time during impulse drying, as shown in Fig. 11. Over a time interval of 40 ms the temperature at the interface between the ceramic and the steel layers at e remained constant and equal to the temperature on the heated side of the steel platen at f. This result implied that heat transfer to the sheet of paper was entirely from the ceramic coating and that the infinite thickness assumption was valid.

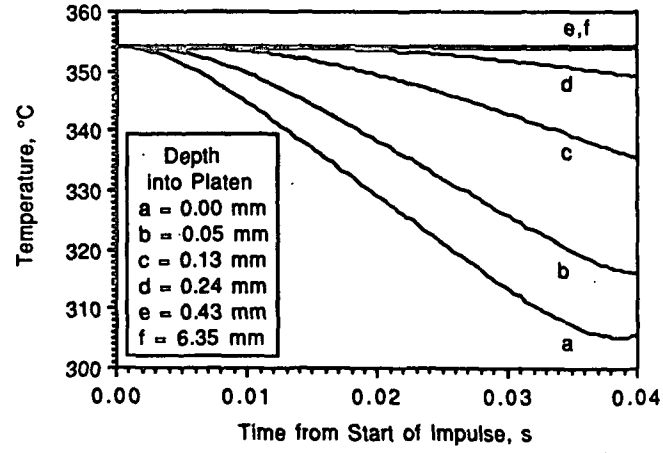

Figure 11. Predicted temperature profiles in the ceramic coated steel platen during impulse drying.

Comparison Of Heating Modes

Infrared and induction heating modes were investigated in terms of internal roll temperature profiles and heating efficiency at a commercial linear roll speed of 760 m/min. In each of the simulations, an ingoing roll surface temperature of 370°C was assumed.

To investigate the influence of roll internal temperature, an oil temperature of 148°C was chosen as a conservative lower limit while 315°C was chosen as an upper limit. Fig. 12 and 13 show temperature profiles for the infrared heating mode at 148°C and 315°C, and Fig. 14 and 15 show profiles for the induction heating mode. Profiles at various locations around the roll were chosen as defined in Fig. 1.

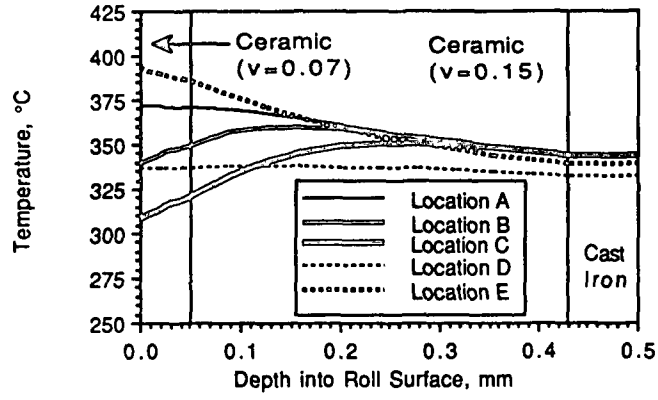

Figure 12. Roll temperature profiles for the case of infrared heating assuming an internal roll temperature of 148°C.

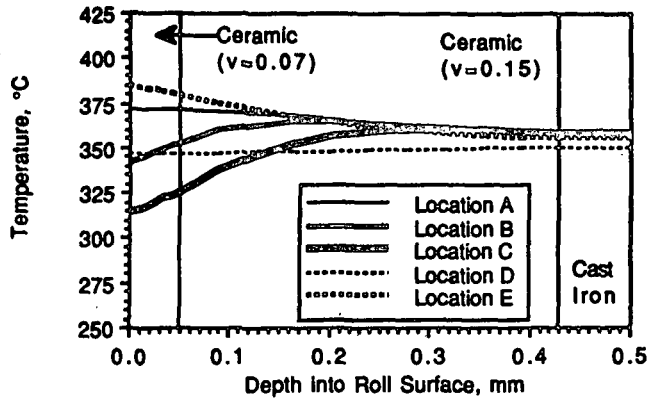

Figure 13. Roll temperature profiles for the case of infrared heating assuming an internal roll temperature of 315°C.

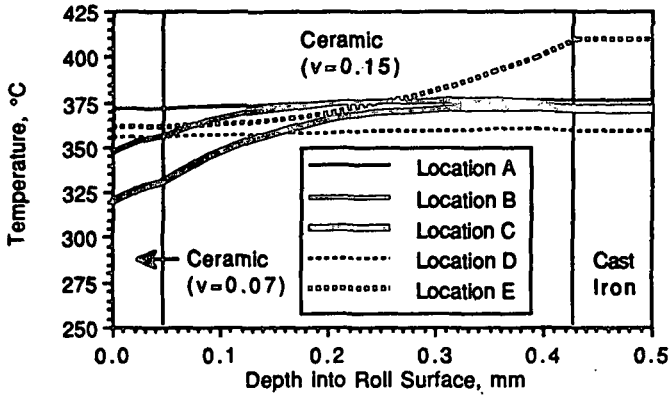

Figure 14. Roll temperature profiles for the case of induction heating assuming an internal roll temperature of 148°C.

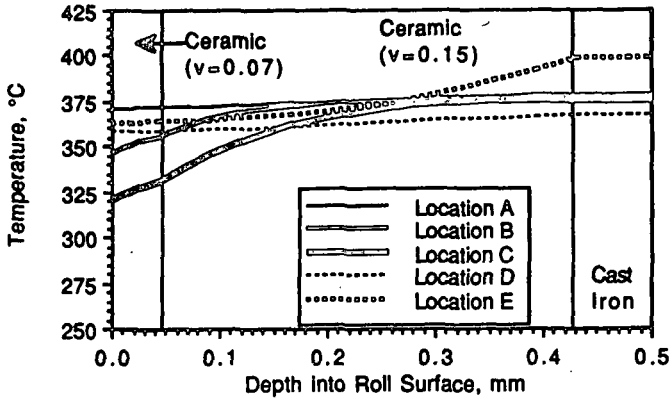

Figure 15. Roll temperature profiles for the case of induction heating assuming an internal roll temperature of 315°C.

The durability of the roll coating will increase if temperature fluctuations at the ceramic/cast iron boundary are minimized. For the infrared case, where energy is supplied at the roll surface, these fluctuations were held to less than 10°C during the time that the roll moved through the heating zone from location D to location E. For the induction heating case, temperature fluctuations of the order of 30 to 50°C were predicted. From a coating durability standpoint the present two layer zirconium oxide ceramic coating is well suited to infrared heating but may be less suitable for induction heating.

The simulations were also used to examine energy losses to the external ambient environment and to the internal heat transfer medium. Fig. 16 shows the distribution of energy transferred to the roll. Using an infrared energy source a maximum of 31 kJ/m^2 must be transferred to the roll. If the system can be designed for higher oil temperatures, as little as 19 kJ/m^2 will be required.

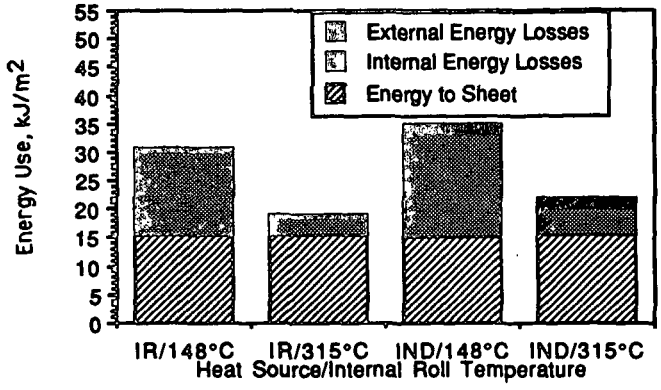

Figure 16. Distribution of energy transferred to the roll.

Fig. 17 shows the same information in terms of roll heating efficiency, defined as the percentage of the energy used to heat the roll that is actually transferred to the sheet. Here again the advantages of operating at higher oil temperature are clearly apparent.

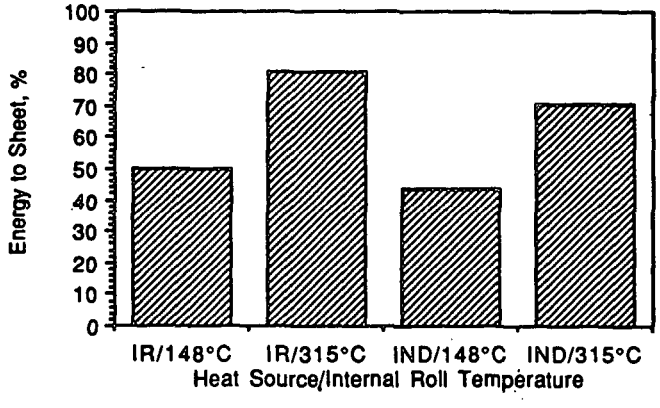

Figure 17. Roll heating efficiency.

Conclusions

A number of process and design issues have been addressed in this work. Roll durability is expected to improve when cyclic temperature fluctuations at metal-ceramic boundaries are minimized. The simulations show that the magnitude of these fluctuations are dependent on the location within the roll where heat is applied. In addition, the energy efficiency of the process has been shown to depend on the internal temperature of the roll as well as the mode of heating.

From a process design standpoint, the simulations were used to estimate the energy requirements of the process and to demonstrate that further research is needed to develop an optimum ceramic coating for induction heating.

Acknowledgements

The work reported was supported by the member companies of the Institute of Paper Science and Technology and by the U.S. Department of Energy Office of Industrial Programs through Grant No. DE-FGO2-85CE40738. Their support is gratefully acknowledged.

References

Batakis, A.P., and Vogan, J.W., 1985, "Rocket Thrust Chamber Thermal Barrier Coatings," NASA CR-175022.

Carnahan, B., Luther, H. A., and Wilkes, J. O., 1969, "Applied Numerical Methods," Wiley, New York.

Crouse, J.W., Woo, Y.D., and Sprague, C.H., 1989, "Delamination-A Stumbling Block To Implementing Impulse Drying Technology For Linerboard," *Tappi Journal*, p.211-215.

Giedt, W.H., 1955, "The Determination of Transient Temperatures and Heat Transfer at a Gas-Metal Interface Applied to a 40-mm Gun Barrel," *Jet Propulsion*, Vol. 25,pp. 158-162.

Hart, P.J., Hsieh, H., and Jones, G.L., 1991, "Simulation of Chlorine Dioxide Substitution," AIChE National Meeting, Los Angeles, Nov. 1991, submitted to *AIChE J.*

Jones, G.L., 1990, "Semi-implicit Method for the Solution of Systems of Stiff Ordinary Differential and Differential-algebraic Equations," *Computers Chem. Engrg.*, Vol. 14, pp. 987-990.

Lavery, H.P., 1988, "High-Intensity Drying Processes-Impulse Drying," Report 3, DOE/CE/40738-T3.

Nanigian, J., "Rocket Igniter Characteristics," Reprinted from Instruments & Control Systems in NANMAC *Temperature Handbook*, Vol. 7, pp. L7-L10.

Nielson, L.E., 1978, "Predicting The Properties Of Mixtures: Mixture Rules In Science And Engineering," Marcel Dekker, New York.

Orloff, D.I., 1992, "Impulse Drying of Linerboard: Control of Delamination," Presented at the 77th Annual Meeting of the Canadian Pulp and Paper Association, to be published in *Journal of Pulp and Paper Science*.

Orloff, D.I., 1991, "Impulse Drying: Controlling Delamination in Heavy Weight Grades," *Institute of Paper Science and Technology Executives' Conference Proceedings*, p.24-27.

Orloff, D.I., 1991, "High-Intensity Drying Processes-Impulse Drying," Report 6, DOE/CE/40738-T6.

Orloff, D.I., and Lindsay, J.D, 1992, "The Influence of Yield, Refining and Ingoing Solids on the Impulse Drying Performance of a Ceramic Coated Press Roll," to be presented at the 1992 Tappi Papermakers Conference

Appendix:

$\beta_0 = 0.12161$ $\quad \gamma_0 = 1.8254 \times 10^{-2}$

$\beta_1 = 1.84 \times 10^{-3}$ $\quad \gamma_1 = -4.6944 \times 10^{-5}$

$\beta_2 = -2.60 \times 10^{-6}$ $\quad \gamma_2 = 9.6 \times 10^{-8}$

$\beta_3 = 1.3277 \times 10^{-9}$ $\quad \gamma_3 = -9.2287 \times 10^{-11}$

$\gamma_4 = 3.1640 \times 10^{-14}$